Two-Dimensional NMR and Restrained Molecular Dynamics Studies of the Hairpin d(T8C4A8): Detection of an Extraloop Cytosine†

Ning Zhou and Hans J. Vogel*

Department of Biological Sciences, University of Calgary, Calgary, Alberta, Canada T2N 1N4

Received June 26, 1992; Revised Manuscript Received October 30, 1992

ABSTRACT: The ^{1}H and ^{31}P NMR resonances of the partly self-complementary 20-mer DNA d(T8C4A8) were assigned by two-dimensional HOHAHA, NOESY, and heteronuclear COSY NMR spectroscopy. The chemical shifts, NOEs, and H–H coupling patterns are indicative of the formation of a hairpin structure with the four C residues forming a loop and the T8·A8 portion of a double-stranded stem. The observation of unusual across-strand NOEs between the A H2 and the T H1′ of the corresponding 3′-end neighboring base pairs of the stem residues suggests that the structure of the hairpin stem deviates from regular B-DNA. A total number of 296 interproton NOEs were used as approximate proton–proton distance constraints in restrained molecular dynamics calculations. Several different starting models, all generated manually from standard B-DNA coordinates, gave rise to virtually the same refined hairpin structure. In the final structure, the interior A-T base pairs of the hairpin stem show a high degree of propeller twist as well as base pair buckle, while the minor groove is slightly narrower compared with a normal B-DNA structure; these features are all common to bent DNA. The first three A-T pairs from the end of the hairpin have a propeller twist and base pair buckle which more closely resemble those of regular B-DNA. The four-residue loop was formed mainly by variations in the phosphate backbone torsion angle ϵ at the loop–stem junctions (residues 8 and 13) and at the first C residue (C 9). The base of the first C residue is positioned outside of the loop. A unique temperature profile of the chemical shifts of the aromatic proton H6 and H5 of the C 9 residue is consistent with the notion that this C base is not stacked in the structure. In addition, the ^{31}P chemical shifts show a good correlation with the backbone torsion angles measured in the refined model.

During the last decade it has become apparent that the structural diversity of nucleic acids extends far beyond the original double helix structure (Watson & Crick, 1953). Hairpin structures, loops, and bulges have been found in nearly all naturally occurring RNA molecules (Rich & Rajbhandary, 1976). In addition, hairpins have also been found in DNA structures, and although they occur much less frequently than in RNA, they probably play an important regulatory role as indicated by the fact that inverted repeat sequences often occur in regions of the DNA associated with biological control (Lilley, 1980; Panayotatos & Wells, 1981; de Boer & Ripley, 1984).

Over the last number of years the structures of a number of DNA hairpins have been determined, in particular by NMR[1] methods (Blommers et al., 1989, 1991; Gupta et al., 1987; Haasnoot et al., 1980, 1983, 1986; Hare & Reid, 1986; Rinkel & Tinoco, 1991; Pramanik et al., 1988; Wolk et al., 1988) but also by X-ray diffraction methods (Chattopadhyay et al., 1988). In general, it has emerged that the stem parts are formed by the complementary Watson–Crick duplexes in either a B-DNA or a Z-DNA structure. Hairpin loops as small as two nucleotides (Orbons et al., 1986; Rinkel & Tinoco, 1991, Ragunathan et al., 1991) or as large as five (Gupta et al., 1987; Williams & Boxer, 1989a,b) have been characterized. While general loop-forming principles have been proposed (Haasnoot et al., 1986; Blommers et al., 1991), it has become evident that the details of loop folding depend on the base sequence in the loop as well as on the adjacent base pairs in the stem (Blommers et al., 1989; Senior et al., 1988; Williamson & Boxer, 1989b), thus generating a rather unique loop structure for each hairpin. In addition, loop structures are also known to influence the structure of the neighboring base pairs in the stem to some degree (Germann et al., 1990).

A rather unusual B-DNA structure is formed by the homopolymer poly(dA)·poly(dT). Of particular interest to us was the propensity of this DNA sequence to bend (Hagerman, 1984, 1990; Wu & Crothers, 1984). This raised the question as to whether this intrinsic bending could be prevented by adding a loop. Conversely, a bent hairpin stem could have profound effects on the loop structure. In this paper, we report a 2D NMR and restrained molecular dynamics investigation of the hairpin structure of the DNA oligomer d(T8C4A8), in which the C4 portion forms a loop. Previous studies on DNA hairpins have largely used loops formed by T residues in which the four unpaired pyrimidine residues form a relatively stable loop, with all four bases positioned inside the loop and partially stacked (Blommers et al., 1991). However, in the hairpin formed by the oligomer d(T8C4A8), we observe that the first loop C base is positioned outside of the loop and is not stacked with other bases. In addition, we find that the hairpin stem has all the expected structural characteristics of the bent A·T-rich DNA.

MATERIALS AND METHODS

The oligonucleotide d(T8C4A8) was synthesized and purified as previously described (Germann et al., 1989). The NMR sample was made up in aqueous 10 mM phosphate

† This research was sponsored by an operating grant from the Medical Research Council of Canada (MRC). H.J.V. is the recipient of a scholarship from the Alberta Heritage Foundation for Medical Research (AHFMR). The NMR facilities were purchased with funds provided by AHFMR and MRC. The molecular graphics equipment was bought through a grant from the Erna and Victor Hasselblad Foundation.

* To whom correspondence should be addressed.

[1] Abbreviations: 2D, two dimensional; COSY, 2D correlated spectroscopy; DQF-COSY, double-quantum filtered 2D correlated spectroscopy; HOHAHA, homonuclear Hartmann–Hahn spectroscopy; NMR, nuclear magnetic resonance; NOE, nuclear Overhauser effect; NOESY, nuclear Overhauser effect 2D spectroscopy.

0006-2960/93/0432-637$04.00/0

buffer solution (pH 7.0) containing 0.1 M NaCl and 0.1 mM EDTA, with a concentration of about 2.5 mM. It was lyophilized several times from 99.9% D_2O before the NMR measurements.

NMR measurements were carried out on a Bruker AM-400 wide-bore spectrometer equipped with an Aspect-3000 computer and on a Bruker AMX-500 spectrometer equipped with an X-32 computer. The temperature was maintained at 15 °C unless otherwise indicated. Pure-absorption phase 2D NMR spectra were obtained using the time-proportional phase incremental method (TPPI). The carrier frequency was set at the residual HDO peak. NOESY spectra were acquired with mixing times of 25, 40, 62.5, 90, 125, and 250 ms; the pulse repetition time was 3.2 s. In order to reduce zero-quantum effects, the mixing times were randomly varied within a range of 5% as proposed by Macura et al. (1981). This appeared to be sufficient; no out-of-phase peaks were observed for any of the sugar protons. Moreover, volume integration of some of the cross peaks counting positive only or both positive and negative data points made no difference in the results. This further indicates that zero-quantum effects were negligible, as has also been shown in a recent study by Wang et al. (1992). A total of 512 FIDs of 2K size with 48 scans each were collected. Multiplication with a 45°-shifted sine-bell and zero-filling were applied in both dimensions before Fourier transformation. DQF-COSY spectra (Rance et al., 1983) were obtained both at 15 and 20 °C; 800 FIDs of 4K size were collected with 48 scans each. Irradiation of the residual HDO peak was used to reduce its intensity. The pulse repetition time was 2 s; again, shifted sine-bell multiplication and zero-filling was applied in both dimensions before Fourier transformation. The final data set consisted of 4K × 2K real points; this gave a digital resolution of 1.2 Hz/point in the t_2 dimension and 2.4 Hz/point in the t_1 dimension. The phosphate-decoupled DQF-COSY spectrum was collected with an inverse probe, using phosphorus broad-band decoupling during acquisition and otherwise the same settings as the DQF-COSY experiments. The HOHAHA experiment was obtained using MLEV-17 spin-lock pulses (Bax & Davis, 1985) and an isotropic mixing time of 65 ms. Data size and processing parameters were similar to those used in the NOESY experiments. The total time for collecting each of the proton 2D experiments varied between 16 and 22 h. The 2D ^1H–^{31}P correlation experiment was recorded at 500 MHz with ^1H detection. The ^1H signal was presaturated with a train of 40 180° pulses spaced by 50 ms during the delay time between consecutive scans (Sklenar et al., 1985). Sweep widths in the F_2 (^1H) and F_1 (^{31}P) dimensions were 8 and 4 ppm, respectively. A total of 160 2K size FIDs were collected with 80 scans each. The total recording time was 9 h.

The NOE cross peaks from the NOESY experiments were categorized into "weak", "medium", and "strong" according to their intensities. The cross peaks labeled "weak" were not clearly defined above noise level at 500 MHz with a 40-ms mixing time. In the 500-MHz NOESY spectrum recorded with 125-ms mixing time, these peaks have 1–2 contour plot levels (the height of two consecutive levels differs by a factor of 2). The cross peaks with 3–4 contour levels were grouped as "medium". Those with 5 or more contour levels were "strong", these could be easily observed at 25-ms mixing time, and these included all the C H5–H6 cross peaks as expected. The 125-ms NOESY spectrum was used for the quantitation of the cross peaks. This is because spin-diffusion effects may become problematic at longer mixing times (James, 1991). Moreover, the potential contributions of zero-quantum coherences become negligible at this mixing time for DNA oligomers of this size, as shown in several recent studies (James, 1991; Wang et al., 1992). Volume integration of a large number of peaks led to the same classification for the cross peaks. For the restrained molecular dynamics calculations, the three groups of NOE cross peaks were converted to approximate proton–proton distance restraints as follows: weak, ≤5.0 Å; medium, ≤3.6 Å; strong, ≤2.8 Å, with a lower limit of 2.0 Å for all of them. The severe overlap of many of the diagonal peaks and cross peaks precluded the use of total relaxation matrix calculations with this hairpin. However, sample calculations for a number of resolved peaks (data not shown) indicated the use of NOE distance constraints as described above to be generally conservative and reasonable.

The software package QUANTA/XPLOR (Polygen Corporation), which was run on a Silicon Graphics IRIS 4D/25 computer, was used to generate and refine the molecular model. For a starting model, we generated the coordinates of a double-helical structure for the sequence T8C2·G2A8 and a double-helical structure for the sequence T8G2·C2A8 from the X-ray crystallographic coordinates of B-DNA (Arnott & Hukins, 1972) with all hydrogen atoms explicitly represented. Then the first strand of the former and the second strand of the latter were combined. The backbone and glycosyl torsion angles of the C residues together with those of the last T and the first A residues were changed interactively, such that a bond was formed between the free 3′-end oxygen of one C and the 5′-end atom P of the other C with reasonable stereochemistry. Starting structures were also generated from T8C3·C1A8, and from T8C1·C3A8 using the same procedure. The empirical energy function developed for DNA by Nilsson and Karplus (1986) was used; this function contains an explicit hydrogen-bond potential. A reduced total charge of –0.32e for the phosphate group (Tidox et al., 1983) and a dielectric constant proportional to the distance (Brooks et al., 1983) were used in calculating the electrostatic potential to stimulate solvent effects. First, the loop together with the A·T pair near the loop were energy minimized to improve the stereochemistry. Subsequently, the NOE constraints were incorporated as a square-well pseudo-energy term $E_{NOE} = \sum K_b T S \Delta^2$, where K_b is the Boltzmann constant, T is the temperature, and S is a scale factor assigned to be 20. Δ is defined as $(\gamma - d_+)$ when $\gamma > d_+$, as 0 when $d_- < \gamma < d_+$, as a $(d_- - \gamma)$ when $\gamma < d_-$; γ is the distance between the two protons that are involved in an NOE interaction. The upper limit d_+ was determined from the NOE cross peak intensity (see above), and the lower limit (d_-) was 2 Å for all distance constraints. Distance constraints for hydrogen bonding between the A·T base pairs were also included.

In the calculations, 100 steps of energy minimization with the Powell algorithm (Powell, 1977) were followed by a 12.5-ps dynamics calculation (in 0.001-ps steps) at constant temperature (300 K) in which the velocities were rescaled to 300 K every 0.1 ps. The structures from the last 2.5-ps dynamics calculation were averaged, and the averaged structure was subjected to additional energy minimization (Nilges et al., 1987). A nonbonded interaction cutoff distance of 11.5 Å was used with a cubic switching function between 9.5 and 10.5 Å. In the dynamics calculation, the Verlet integration method (Verlet, 1967) was used with initial velocities assigned from a Maxwellian distribution at 300 K. The calculation procedure to refine one starting model required approximately 4 h of cpu time on the Iris 4D/25.

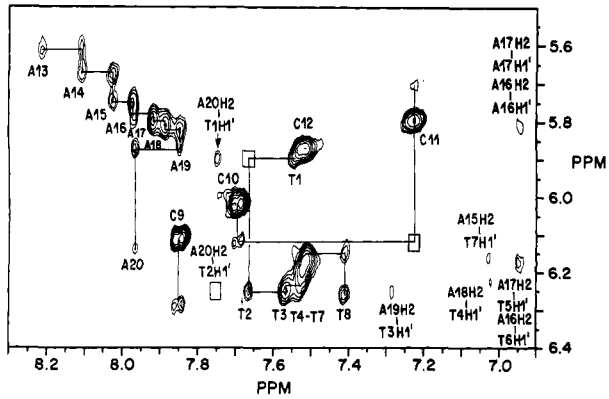

FIGURE 1: Region of the contour plot of the 400-MHz proton NOESY spectrum (mixing time = 250 ms) of d(T8C4A8) showing cross peaks between the base aromatic protons and the sugar H1′ protons. The squares indicate weak cross peaks which could only be identified at a lower contour level. The intraresidue and interresidue H8/H6–H1′ cross peaks for T and A used to make the sequential assignments were connected by a line, and the intraresidue cross peaks were labeled with the appropriate residue names. A strong cross peak between the loop C residue H5 and H6 protons (labeled with residue name) and a weaker intraresidue H6–H1′ cross peak were observed (in the case of C12, this overlaps with the H6–H5 cross peak). However, no interresidue base–H1′ NOE peaks between the T8 and the C9, between the C residues (except a very weak C11 H6–C10 H1′), and between the C12 and the A13 were detected.

RESULTS

Proton NMR Assignments. The oligonucleotide d(T8C4A8) undergoes a structural transition in aqueous solution at 45.7 °C which can be monitored by UV absorption at 265 nm. The transition temperature was shown to be independent of concentration, suggesting that the structure formed by d(T8C4A8) below 45.7 °C is a monomolecular species (Germann et al., 1989). Given the sequence of the oligonucleotide, we expect it to be able to form a hairpin structure. In order to work with only one stable structure, the proton NMR experiments were recorded at 15 and 20 °C.

The proton NMR assignments of the nonexchangeable protons were obtained through the combined use of 2D HOHAHA and NOESY experiments. In the HOHAHA spectrum, cross peaks between sugar protons of the same nucleotide were analyzed in three groups: the first one included H1′, H2′, H2″, and H3′; the second one includes H3′ and H4′; and the third group contains the H4′, H5′, and H5″ protons. With an isotropic mixing time of 65 ms, multistep magnetization transfer was not effective between the H3′–H4′ coupling; however, this allowed for the unambiguous identification of the H3′ and the H4′ protons. All the sugar protons from each nucleotide could be identified in this manner. They were subsequently connected through the use of NOESY spectra. The H6 and the H5 protons of each of the four cytosine residues could all be connected by a HOHAHA cross peak between them. Sequence-specific assignments were obtained from NOESY spectra following established procedures (Scheek et al., 1984; Hare et al., 1983). Figure 1 shows an expansion of the NOESY contour plot of the base proton–H1′ region. Both the intraresidue $H8(6)_i$–$H1'_i$ and the interresidue $H8(6)_{i+1}$–$H1'_i$ cross peak were observed within the T8 and the A8 fragments, making the sequential assignments possible for both strands of the stem. However, the interresidue base–H1′ cross peaks between T8 and C9, between C12 and A13, and between the consecutive C's were not detected [except for a weak C11 H6–C10 H1′ cross peak (Figure 1)], which indicates poor base stacking between the corresponding residues. Consequently, information from other regions of the NOESY spectra needed to be used to complete the sequential assignment in the loop region. Interresidue base–H2″ (or H2′) NOEs for the loop C residues were also not observed. Moreover, the intraresidue $H6(8)_i$–$H3'_i$ and interresidue $H6(8)_{i+1}$–$H3'_i$ cross peaks of the T's and A's nearly overlap (Figure 2, left). However, the intra- and interresidue cross peaks involving C H6–H3′ and H5–H3′ were well resolved (Figure 2) and afforded the sequential assignments of the residues. Among them the C11 H6–C10 H3′ and the C11 H5–C10 H3′ peaks are more intense; while the C12 H5–C11 H3′ is very weak, and no C12 H6–C11 H3′ was detected. A weak cross peak between the A13 H8 and the C12 H3′ (Figure 2, left) connects the C and A fragments and provides further support for the sequential assignments of the C residues. No cross peaks between the C9 and the T8 protons were detected.

The A H2 proton is not scalar-coupled to any other proton and is therefore not grouped by the HOHAHA experiments. NOESY cross peaks between adjacent A H2 protons (Figure 3) were used to connect them in order. Weak cross peaks to the H1′ of the same A residue and to the T H1′ protons of the opposite strand were detected for some of the A H2 protons (Figure 1), which provided the necessary information to fit the A H2 protons into the sequential assignments. The complete proton resonance assignments are summarized in Table I.

Phosphorus NMR Assignments. In DNA, each phosphorus atom is three bonds removed from the H3′ proton of one sugar residue and four and three bonds away, respectively, from the H4′ and H5′/H5″ protons of the next residue. The phosphorus NMR signals can be correlated to these proton signals through heteronuclear COSY experiments (Figure 4). The phosphorus resonances of d(T8C4A8) could thus be assigned on the basis of the proton assignments. The cross peaks involving the loop C residues are well resolved. In addition to providing the complete assignment of the ^{31}P NMR spectrum, this experiment provided a confirmation of the loop proton sequential assignments. For all the C residues, we noted that the intensity of the P–H4′ cross peak is lower than that of the P–H5′ (H5″) cross peak; in addition, the P–H3′ cross peak is always the strongest. The residues in the middle of the stem have very similar ^{31}P chemical shifts (within a range of 0.2 ppm) and almost identical H3′ (as well as H4′, H5′, H5″) chemical shifts. This is an indication that, at the middle of the hairpin stem, the residues are very similar in nature (see below).

Deoxyribose Ring Conformation. The H1′–H2″ and H1′–H2′ cross peaks of the A and C residues are resolved in the DQF-COSY experiment, thus allowing an assessment of their deoxyribose ring conformation (Figure 5). The outer splittings of the H1′ signals measured along the F_2 dimension vary between 15 and 20 Hz. Their cross peak pattern is indicative of a small H1′–H2″ and a large H1′–H2′ coupling constant (Figure 5), which is characteristic of a C2′-endo sugar ring conformation (Rinkel & Altona, 1987). Other features, including weak H3′-H4′ cross peaks and the absence of H3′–H2″ cross peaks, are also consistent with a predominantly C2′-endo conformation for the deoxyribose ring (Rinkel & Altona, 1987). The signal overlap for the T residues is quite extensive. However, the cross peaks for T1, T7, and T8 are partially resolved, and their patterns indicate that the deoxyribose rings of these nucleotides are also mainly in the C2′-endo conformation.

Temperature Study. The temperature dependence of the chemical shifts of the base H5 and H6 proton resonances from the four-loop C residues was studied by recording

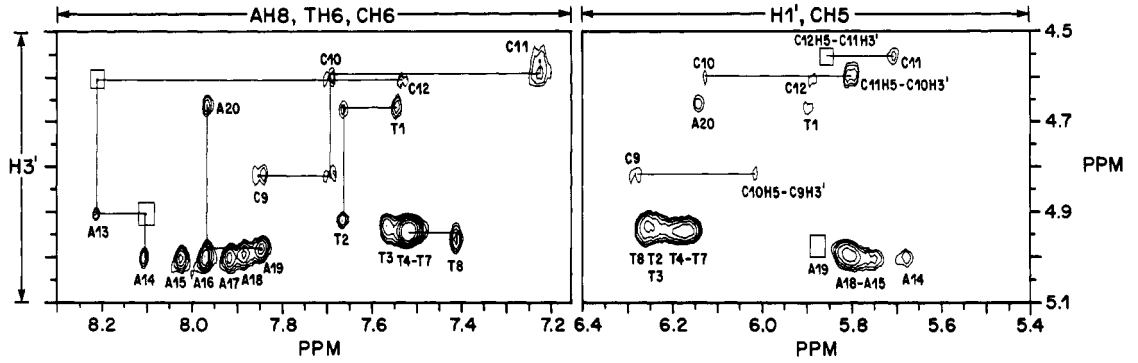

FIGURE 2: Regional contour plots of the 400-MHz NOESY experiment (mixing time = 250 ms) showing cross peaks between the H3′ and the H8/H6 protons (left panel) and between the H3′ and the H1′/H5 protons (right panel). Intraresidue H8/H6–H3′ cross peaks in the left panel and the H1′–H3′ cross peaks in the right panel were labeled with residue names. Resolved interresidue H8/H6–H1′ peaks were connected with lines in the left panel. These NOE peaks help give complete sequential assignments of the loop C residues. Several observed interresidue H5–H3′ cross peaks provide an extra check of the assignments and were labeled in the right panel.

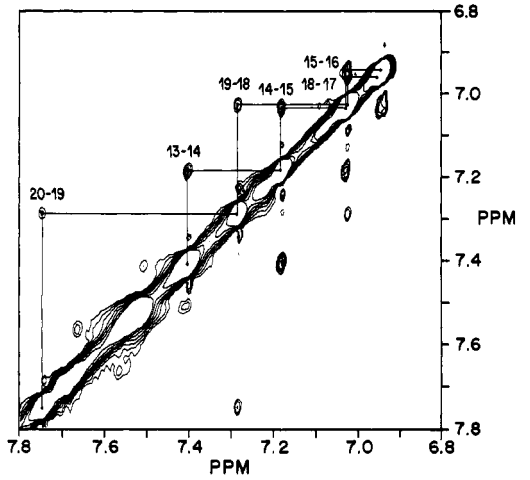

FIGURE 3: Regional contour plot of the 400-MHz NOESY spectrum (mixing time = 250 ms) of d(T8C4A8) showing cross peaks between the H2 protons of adjacent A residues. Cross peaks are labeled with the two residue numbers corresponding to the H2 protons that are connected by the cross peak. Cross peaks with lower intensities between the H6 protons of adjacent T residues are also shown but not labeled.

NOESY and HOHAHA spectra at temperatures ranging from 10 to 70 °C. The averaged melting point of these aromatic protons is 46.6 °C (Figure 6), which is in good agreement with the melting point determined by UV spectroscopy (Germann et al., 1989). The concentration range convered by the UV study was 3.8–120 μM. The melting point measured from the C base proton NMR signals of a 100 μM sample was within 0.2 °C of the result measured from the 2.5 mM sample. Furthermore, around this transition temperature, the chemical shifts of the H6 and H5 protons of the C9 base move in an opposite direction to the base protons of the three other bases. This strongly suggests that the C9 base is not stacked in the hairpin loop structure; therefore, the characteristic downfield shift caused by the loss of base stacking during melting is not observed for this base. In contrast, the three other loop C bases display the characteristic downfield shift during the hairpin to coil transition. The relative downfield resonance positions of the H6 and H5 protons of the C9 in the hairpin, compared with other C residue base protons, also reflect the lack of an upfield ring-current shift which would have been induced by base stacking. With temperatures above the melting point, the chemical shifts of the H5 and the H6 protons of all the C residues approach a common value; this reflects a partially stacked C base in a random coil single-strand state. The small downfield shifts in the H5 and the H6 protons of the C9 base in the hairpin relative to the denatured form can then be interpreted tentatively as going from a partially stacked position to an unstacked position when the hairpin is formed. Therefore the temperature profile is consistent with the presence of an unstacked C9 base in the hairpin.

Measurement of ^{31}P–H3′ Coupling Constants. In the DQF-COSY spectrum, the separation of the outer peaks of the H3′–H2′ cross peaks along the H3′ region in the F_2 dimension results from $J_{H3'-H2'} + J_{H3'-H2''} + J_{H3'-H4'} + J_{P-H3'}$. This separation for the C residues is 15–16 Hz. In the DQF-COSY spectrum recorded with ^{31}P broad-band decoupling, the separation reduced to 9–10 Hz. By subtracting the latter from the former, an estimate of the three-bond $J_{P-H3'}$ was obtained. For the loop C residues, the following $J_{P-H3'}$ values were deduced: C9, 6.7 Hz; C10, 6.0 Hz; C11, 6.3 Hz; and C12, 6.0 Hz. Signal overlap prevented us from making similar measurements for the T and A residues, with the exception of the $J_{P-H3'}$ for T1 which was estimated as 2.5 Hz.

The $J_{P-H3'}$ is related to the backbone torsion angle ϵ by a Karplus-type equation: $J = 15.3\cos^2\theta - 6.1\cos\theta - 1.6$, where $\epsilon = \theta + 120°$ (Lankhorst et al., 1984). One J value can correspond to up to four ϵ values. While it seems reasonable to choose ϵ for the T1 residue to be close to the ϵ value found in typical B-DNA crystal structures [−150° to −200° (Arnott & Hukins, 1972)], the loop residues and the residues at the loop–stem junctions could display a wider range of ϵ torsion angles. The possible values of ϵ which can be deduced from these $J_{P-H3'}$ values are discussed below in relation to the ϵ torsion angles measured in the NOE restrained molecular dynamics structure.

NOE Restrained Molecular Dynamics Structure. The proton NMR NOE data not only provide the sequential assignments (see above) but they also identify short-distance proton–proton pairs, and therefore they define the three-dimensional molecular structure. A qualitative analysis of the NOESY spectra of d(T8C4A8) shows that the general NOE cross peak patterns observed for the T8–A8 part are consistent with a B-DNA type of structure. However, the A H2–T H1′ NOEs between the two strands (Figure 1) are not normally observed for a standard B-DNA structure (Scheek et al., 1984). The interruption of the interresidue base–H1′ NOEs between the C residues, between the A and C, and between the C and T indicate decreased base stacking in the loop and at the loop–stem junctions. Based on these qualitative observations, several hairpin models were built for d(T8C4A8) with a stem consisting of eight T·A base pairs and a loop consisting of four C residues (see Materials and Methods). A total of 296 NOEs (Table II) were converted to approximate

Table I: Proton Chemical Shifts[a] of d(T8C4A8)

	H6/H8	H5/H2/CH3	H1′	H2′	H2″	H3′	H4′	H5′, H5″
T1	7.54	1.61	5.90	2.24	2.59	4.68	4.13	3.77
T2	7.66	1.68	6.25	2.35	2.66	4.92	4.30	4.10
T3	7.57	1.64	6.23	2.32	2.70	4.93	4.30	4.10
T4	7.53	1.64	6.20	2.32	2.70	4.95	4.34	4.28, 4.18
T5	7.52	1.64	6.18	2.32	2.70	4.95	4.34	4.25, 4.16
T6	7.52	1.64	6.18	2.32	2.70	4.95	4.34	4.25, 4.16
T7	7.51	1.69	6.15	2.15	2.60	4.95	4.34	4.22, 4.15
T8	7.41	1.70	6.26	2.31	2.43	4.97	4.24	4.16
C9	7.85	6.10	6.28	2.23	2.47	4.82	4.34	4.12
C10	7.68	6.02	6.12	2.03	2.27	4.60	4.10	4.00, 3.85
C11	7.22	5.79	5.70	1.77	2.29	4.57	3.81	3.78, 3.60
C12	7.52	5.87	5.87	1.96	2.24	4.62	4.10	3.85
A13	8.21	7.40	5.62	2.62	2.70	4.91	4.27	3.98, 3.92
A14	8.10	7.18	5.68	2.61	2.76	5.01	4.36	4.16
A15	8.02	7.02	5.75	2.55	2.79	5.01	4.36	4.17
A16	7.96	6.92	5.78	2.46	2.85	5.00	4.42	4.22
A17	7.92	6.93	5.80	2.44	2.85	5.00	4.40	4.22
A18	7.88	7.02	5.82	2.42	2.85	4.99	4.40	4.22
A19	7.84	7.27	5.87	2.40	2.82	4.98	4.40	4.22
A20	7.96	7.73	6.14	2.36	2.49	4.67	4.24	4.16

[a] Chemical shifts are reported in parts per million relative to the internal standard TSP at 15 °C in phosphate buffer solution (pH 7.0). The chemical shifts of the H5′ and H5″ protons are less accurate; when their chemical shifts are inequivalent, no distinction was made between H5′ and H5″.

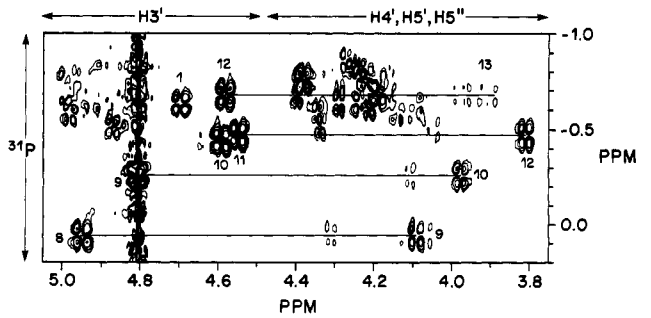

FIGURE 4: Contour plot of a proton-detected pure absorption mode 2D ^{1}H–^{31}P correlation spectrum of d(T8C4A8). Both positive and negative contour levels are plotted. Experimental details are given under Materials and Methods. Shown on the x-axis is the H3′, H4′, H5′, and H5″ proton resonance region; along the y-axis are the phosphorus resonances. A horizontal line at the chemical shift position of each resolved P connects the P–H3′ cross peak on the left side and the P–H4′ and P–H5′ (H5″) cross peaks on the right side. Labels indicate the residue number that the corresponding protons belong to.

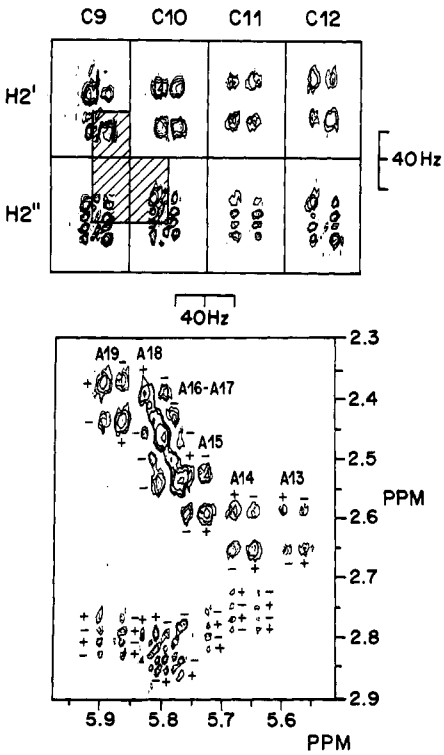

FIGURE 5: (Upper) H1′–H2″ and H1′–H2′ cross peaks of the loop C residues of a 500-MHz DQF-COSY spectrum of d(T8C4A8). The areas enclosed in the shadowed region overlap with other cross peaks. The experimental details of the 2D spectrum are given under Materials and Methods. (Lower) Regional contour plot from the same DQF-COSY spectrum showing the cross peaks between the H1′ and the H2′ and between the H1′ and the H2″ protons of the A residues (except A20). Positive and negative contour levels are indicated by + and – signs, respectively.

proton–proton distance restraints according to their intensities. These include 53 distances for the loop and loop–stem junction area and 243 distances for the stem part. The NOEs involving H5′ and H5″ protons and T methyl protons were not used as constraints because of the lack of stereospecific assignments and because of possible complications due to extra motions of the methyl groups. Weak NOEs that were only detected with mixing times longer than 125 ms were also not used as distance contraints, because increasing spin-diffusion at longer mixing times can give erroneous results. There is extensive chemical shift degeneracy for the same type of proton in the T residues in the middle of the stem (T4–T6). This is true to a lesser extent for the A residues. Judging from their chemical shifts and from the resolved intra- and interresidue NOEs, the middle A·T base pairs display quite uniform conformations. Therefore the same constraints were used for the four middle T and for the four middle A residues. The starting models were subjected to restrained molecular dynamics calculations as described under Materials and Methods. The different starting models gave rise to virtually the same refined structures. In the refined structure, all of the NOE distance violations greater than 0.1 Å were eliminated, which were primarily from the loop residues and the loop–stem junction residues (10–14 out of a total number of 14–18 for starting models). The rmsd between the corresponding distances in the refined structure and the NOE constraints is 0.006. In all the starting models, the C9 residue was positioned inside the loop, like the rest of the C residues. However, in the refined models, the C9 base is extraloop (Figure 7). Apparently, the approximate distance constraints used were able to restrain the structure such that is became consistent with the unusual temperature profile of the C9 aromatic protons.

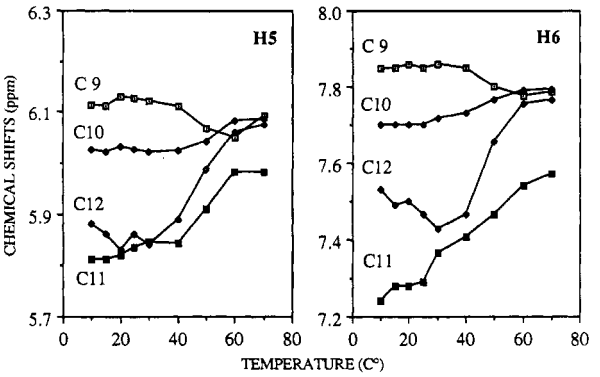

FIGURE 6: Chemical shifts of the loop C aromatic protons are plotted (H5, left panel; H6, right panel) against the experimental temperatures. The residue numbers are labeled beside each curve.

Interpretation of ^{31}P NMR Data. It has been reported that the ^{31}P chemical shifts of DNA oligonucleotides are mainly affected by the backbone torsion angle ϵ. A downfield-shifted ^{31}P signal is usually related to an abnormal ϵ and therefore to a higher energy form (Powers et al., 1990). The backbone torsion angles ϵ measured in the refined structure of d(T8C4A8) correlate well with their ^{31}P chemical shifts (Figure 8). Like their proton chemical shifts, the phosphorus chemical shifts of the T and A residues in the middle of the stem are nearly identical, and hence they display fairly uniform ϵ angles (−180 to −190°) (though T4 is an exception). The ϵ torsion angles of T8 (−138°), C9 (−85°), and A13 (−99°) deviate substantially from the ϵ values in the rest of the molecule. Their ^{31}P chemical shifts are indeed more downfield-shifted (Figure 8), although the order is reversed for T8 and C9. The ϵ angles of the residues 1, 4, 10, and 11 are relatively small, compared to the majority of the stem residues. In order to further analyze the backbone angle deviations, the torsion angles ϵ are plotted against ζ in Figure 9. The straight line gives the correlation of these two angles found for typical B-DNA structure ($\zeta = -367 - 1.54\epsilon$) (Powers et al., 1990). The ϵ–ζ correlation of the majority of the stem residues (residues 2, 3, 5–7, 14–16, 18, and 20) are very close to the line and fall in a small area for a low-energy B conformation defined as BI (Dickerson, 1983). The loop residue C9 displays substantially smaller ϵ and smaller ζ as well. The C10 and C11 correlations are both apparently outside the BI region, yet C12 has "normal" BI ϵ and ζ angles. The correlation for the A13 at one loop–stem junction is in the area defined as BII. The T8 at the other loop–stem junction displays ϵ–ζ angles near the BI area. Residues 4 and 17 among the stem residues display a ϵ–ζ correlation that deviates clearly from the BI area. The sugar ring pseudorotation phase angle P does not display significant variation. It appears that, to form the stable hairpin structure, the largest distortion occurs to the backbone angles ϵ and ζ and the glycosidic angle χ at T8, C9, and A13.

The estimated ^{31}P–H3′ coupling constants of C10 and C11 (6.0–6.3 Hz) are consistent with the smaller ϵ angles in the model. However, the ϵ of C12 (−178°) corresponds to a smaller ^{31}P–H3′ coupling constant (2.2 Hz), and the ϵ of C9 (−85°) corresponds to a larger constant than the estimated values. The value for the T1 residue (2.5 Hz) is consistent with ϵ angles in the BI area and with the model. Given the low accuracy in measuring the coupling constants and the uncertainty of choosing the ϵ for the loop and junction residues, the available loop torsion angle constraints were not used in the molecular dynamics calculation.

DISCUSSION

Intrinsic DNA helix bending and bendability have been recognized as important recognition features for sequence-specific protein–DNA binding (Travers, 1989). Oligo(dA)·oligo(dT) tracts have been shown by a variety of techniques to cause DNA helix bending [for a review, see Hagerman (1990)]. X-ray crystallography (Nelson et al., 1987; Yoon et al., 1988) and NMR spectroscopy studies (Behling et al., 1987; Nadeau & Crothers, 1989; Katahira et al., 1988, 1990) of various DNA duplexes containing oligo(dA)·oligo(dT) tracts have shown that their structures are different from a standard B-DNA. The bend DNA features a narrower minor groove, a high propeller twist, and a large base pair buckle compared to standard B-form DNA. The existence of bifurcated hydrogen bonds between adjacent base pairs, which would stabilize the high propeller twist, has also been suggested on the basis of the X-ray crystallography studies. The presence of this type of hydrogen bond was noted in a recent molecular dynamics simulation of poly(dA)·poly(dT) (Fritsch & Westhof, 1991), and the term "three-center" hydrogen bond was used. These atypical structural features cause an overall bending of the DNA helix.

The MD-refined hairpin structure in Figure 7 determined for d(T8C4A8) shows some evidence for DNA bending in the stem as well as for an unusual loop structure. These two aspects will be discussed separately below. For the four A·T pairs in the middle of the stem, the proton chemical shifts and proton NOE and COSY patterns as well as ^{31}P chemical shifts are nearly the same. Since these residues are almost free from end effects and from the effect of the loop formation, they are expected to be nearly polymeric in character. Indeed, their proton chemical shifts and NOEs are very similar to those reported for poly(dA)·poly(dT) (Sarma et al., 1985; Behling & Kearns, 1986) and for non-end residues of the $(dA)_{10}$·$(dT)_{10}$ duplex (Behling et al., 1987). The observed cross-strand NOEs between A H2s and the corresponding T H1′ of their neighbor base pairs (toward the loop direction) are approximately twice as intense as the intraresidue A H2–A H1′ NOEs [Figure 1; see also Behling and Kearns (1986) and Nadeau and Crothers (1989)]. All the central A·T base pairs display a high propeller twist (average 19°) and base pair buckle (average 22°). The three base pairs near the stem free end have more normal values of propellar twist (8°) and base pair buckle (7°). This discontinuous behavior has been noted before in A·T duplexes (Nadeau & Crothers, 1989). The average phosphate–phosphate distance measured in the model in the minor groove is 10.9 Å. This is about 0.6 Å lower than the value obtained in regular B-DNA. Thus, the stem of the d(T8C4A8) hairpin displays all the structural features which have been reported for other bent A·T-rich duplexes.

Our NOE data demonstrate the proximity between the A H2 and the 3′-end base pair TH1′ on the other strand. The higher propeller twist and high base pair buckle of the internal A·T base pairs of the refined structure cause A H2 and T H1′ of the 3′-end base pair to be within ~3.8 Å of each other; this is well within the NOE-detectable range. This feature also brings the A amino proton (N6-H) closer to the T O4 of the 3′-end base pair (~3.2–3.5 Å), compared with the corresponding distance of ~4.4 Å in a B-DNA structure. The possible transient formation of three-center hydrogen bonds involving A N6H and T O4 (Fritsch & Westhof, 1991) can be attributed to this proximity. In the refined model the helix axis of the stem (excluding the three base pairs at the end) appears to be bent toward the major groove side. However, since the NOE measurement identifies short distances only

Table II: Proton NOEs of d(T8C4A8) Used in the Restrained Molecular Dynamics Calculations[a]

	intraresidue											
residue no. (*i*)	H8/H6 | H1′	H8/H6 | H2′	H8/H6 | H2″	H8/H6 | H3′	H8/H6 | H4′	H1′ | H2′	H1′ | H2″	H1′ | H3′	H1′ | H4′	H3′ | H2′	H3′ | H2″	H3′ | H4′
1	+	+++	+	+	+	+	+	+	++	+	+	+++
2	+	+++	+	+	+	+	+++	+	++	+++	+++	+++
3–6	+	+++	+	+	+	++	+++	+	++	+++	+++	++
7	+	+++	+	+		++	+++	+	++			++
8	+	+++	+	+		++	+++	+	++			++
9	+	+++	+	+		++	+++	+	+	+++	++	++
10	+	+++	+	+		++	+++	+	+	+++	++	++
11	+	+	+	+		++	++	+	+	+++	++	++
12		+	+	++		++	+++	+	+	+++	++	++
13	+	+++	+	+		++	++			+++	+++	++
14	+	+++	+	+	+	++	+++	+	++	+++	+++	++
15–18	+	+++	+	+	+	++	+++	+	++	+++	+++	++
19	+	+++	+	+	+	+	+++	+	++	+++	+++	++
20	+	+++	+	+	+	+	+++	+	++	+++	+++	++

	interresidue [(*i*) – (*i* – 1)]								
residue no. (*i*)	H8/H6 | H1′	H8/H6 | H2′	H8/H6 | H2″	H8/H6 | H3′	H5 | H3′	H5 | H1′	H5 | H2′	H2 | H2	H2 | T(22 – *i*)H1′
2	+	+	+	+					
3–6	+	+	+	+					
7	+	+	+	+					
8	+		+	+					
9									
10			+	+	+				
11	+			+	+	+	+		
12									
13			+	+					
14	+		+					+	
15–18	+	+	+					+	+
19	+	+	+					+	+
20	+	+	+					+	+

[a] The symbols +, ++, and +++ indicate weak, medium, and strong NOEs observed between the corresponding protons, respectively. See Materials and Methods for details of classifying the NOE intensities.

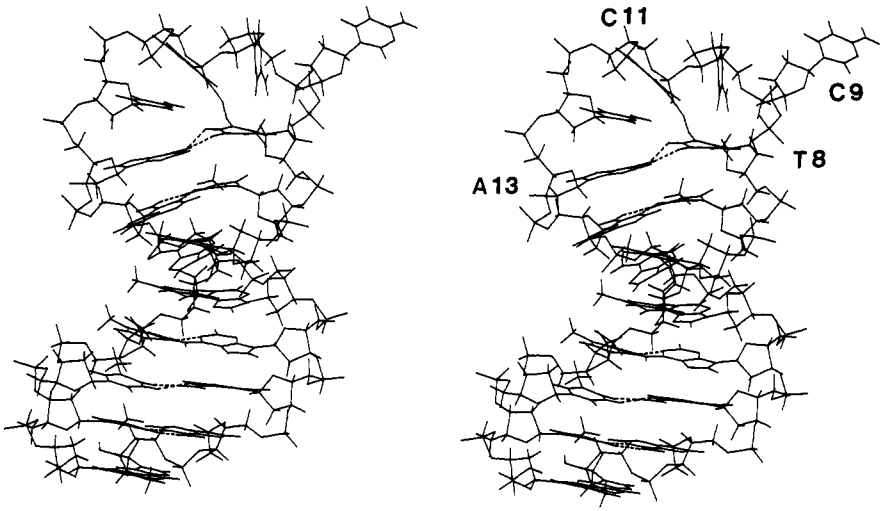

FIGURE 7: Restrained molecular dynamics structure of the d(T8C4A8) hairpin represented as a stereopair. Hydrogen bonds are indicated by dashed lines. Note the extraloop position of C9 and the hydrogen bond formed between the T8 O2 and the C11 H4 2.

(<5 Å), it is only sensitive to local structural features, and hence it does not provide direct evidence of more long-range helix bending. Indeed, the NOE cross peak patterns observed for the bent stem are largely consistent with normal B-DNA, with the exception of the observation of interstrand NOE.

Our NMR data and modeling of the (T8C4A8) hairpin demonstrate that the deoxyribose ring conformations of the stem residue and the loop residues are not significantly different. All of them are primarily in the C2′-endo conformation, and hence loop formation is not accompanied by unusual deoxyribose structures as has been noted before for most other DNA hairpins (Blommers et al., 1991). The loop formation appears to be achieved mainly by a variation of the backbone angle ϵ. In particular, the ϵ of the two closing residues of the stem (T8 and A13) and to a lesser extent the ϵ of the loop C9 residue are altered. The measured ^{31}P chemical shifts for the backbone are in good agreement with the model. The base stacking in the loop between the C10 and C11 bases is

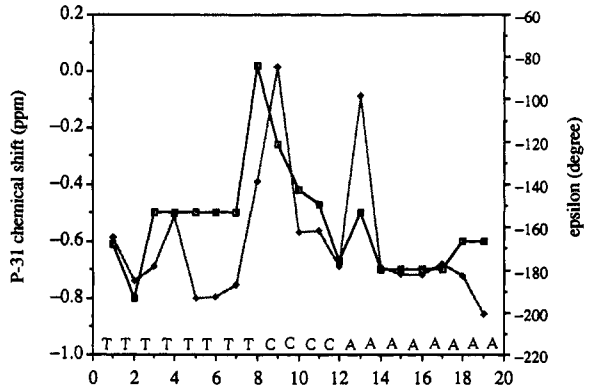

FIGURE 8: ^{31}P chemical shifts (□) and backbone torsion angle ϵ (◆) of the restrained molecular dynamics model of d(T8C4A8) are plotted against residue numbers.

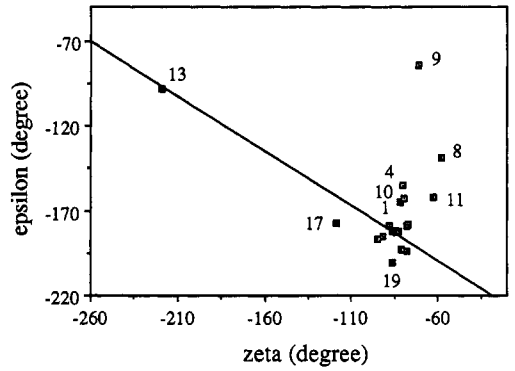

FIGURE 9: Correlation of the backbone torsion angles ϵ and ζ of the restrained molecular dynamics model. The straight line represents the best linear correlation ($\zeta = -367.5 - 1.54\epsilon$) obtained from crystallographic B-DNA structure. The positions for residues 2–7, 12, 14–16, 18, and 20 are clustered in a small area which is defined as the BI conformation (Dickerson, 1983). Labeled with residue numbers are the correlations for three of the four loop C residues and the two loop–stem junction residues 8 and 13, which are outside of this area. Residue 13 falls in the area defined as BII. Residues 4 and 17 also deviate from the BI area, representing a discontinuity between the three A·T pairs at the free end of the hairpin and the interior A·T pairs.

weaker than the stacking between the stem residues. Base stacking between C11 and C12 and between C12 and A13 is even weaker. This general stacking pattern is inconsistent with a model for loops with four bases which proposes continued stacking in the 3′-end of the stem, followed by a sharp turn in the sugar–phosphate backbone (Haasnoot et al., 1986).

The structures of more than a dozen DNA hairpin structures with loops of two, three, four, or more pyrimidines have been determined to date (see the introduction). In all cases, the loop pyrimidine bases point inside the loop and experience some degree of base stacking. Hare and Reid (1986) have found a base which is solvent-exposed, but in their case all loop bases are stacked with one another. One recent example has been reported where a loop base folds into the minor groove (Blommers et al., 1991). The hairpin loop structure described for d(T8C4A8) in this paper appears to be quite distinct. We have found that one of the four loop C bases is pointed away from the loop into the solution. This unusual orientation is strongly supported by the observation of the unusual temperature dependence of the chemical shifts for this residue. However, some conformational flexibility of this base is not inconsistent with our data. Since detailed structures for C4 loops have not been reported yet to our knowledge, it is possible that this structure is a peculiarity of such C loops. However, the thermodynamic stability of hairpins with a T4 or a C4 loop and with identical stems is almost indistinguishable (Senior et al., 1988), and hence this premise seems unlikely. Rather we feel that the bent stem structure of the d(T8C4A8) hairpin causes the unusual loop structure. Unstacked bases in DNA have previously been reported for some duplexes (Joshua-Tor et al., 1988; Miller et al., 1988; Morden et al., 1983, 1990; Nikonowicz et al., 1989). In one instance, an unpaired base was demonstrated to adopt an intrahelical conformation in aqueous solution (Roy et al., 1987), but it was extrahelical in the crystal (Miller et al., 1988). Different conformations in solution and in the crystal may also exist for another 15-mer DNA duplex containing unpaired bases (Joshua-Tor et al., 1988). These results indicate the polymorphic nature of the structure that can be adopted by these sequences and their sensitivity to their environment. Be that as it may, our results demonstrate that unstacked bases can occur from loops as well as from duplexes. These unstacked bases would have a greater extent of hydration and would be more accessible to chemical reagents compared with intrahelical and intraloop bases. This can have implications for carcinogenesis and for DNA–protein and DNA–drug interactions. In addition, the high abundance of loops in the structure of RNA suggests that unstacked loop bases could play a role here as well.

ACKNOWLEDGMENT

We thank Dr. H. J. Van de Sande for donating the d(T8C4A8) sample and Dr. N. Pattabiraman for providing one starting model which was calculated by using the program AMBER. Dr. T. L. James kindly provided a copy of the total relaxation matrix analysis program CORMA. We also thank Josie Cleland and Linda Marin for typing the manuscript.

REFERENCES

Arnott, S., & Hukins, D. W. L. (1972) *Biochem. Biophys. Res. Commun. 47*, 1504–1510.

Bax, A., & Davis, D. G. (1985) *J. Magn. Reson. 65*, 355–360.

Behling, R. W., & Kearns, D. R. (1986) *Biochemistry 25*, 3335–3346.

Behling, R. W., Rao, S. N., Kollman, P., & Kearns, D. R. (1987) *Biochemistry 26*, 4674–4681.

Blommers, M. J. J., Walters, J. A. L. I., Haasnoot, C. A. G., Aelen, J. M. A., van der Marel, G. A., von Boom, J. H., & Hilbers, C. W. (1989) *Biochemistry 28*, 7491–7498.

Blommers, M. J. J., van de Ven, F. J. M., van der Marel, G. A., von Boom, J. H., & Hilbers, C. W. (1991) *Eur. J. Biochem. 201*, 33–51.

Brooks, B. R., Bruccoleri, R. E., Olafson, B. D., States, D. J., Swaminathan, S., & Karplus, M. (1983) *J. Comput. Chem. 4*, 187–217.

Chattopadhyaya, R., Ikuta, S., Grzeskewiak, K., & Dickerson, R. E. (1988) *Nature 334*, 175–179.

de Boer, J. G., & Ripley, L. S. (1984) *Proc. Natl. Acad. Sci. U.S.A. 81*, 5528–5531.

Dickerson, R. E. (1983) *J. Mol. Biol. 166*, 419–441.

Fritsch, V., & Westhof, E. (1991) *J. Am. Chem. Soc. 113*, 8271–8277.

Germann, M. W., Vogel, H. J., Pon, R. T., & van de Sande, J. H. (1989) *Biochemistry 28*, 6220–6228.

Germann, M. W., Kalisch, B. W., Lundberg, P., Vogel, H. J., & van de Sande, J. H. (1990) *Nucleic Acids Res. 18*, 1489–1498.

Gupta, G., Sarma, M. H., Sarma, R. H., Bald, R., Engelke, U., Oei, S. L., Gessner, R., & Erdmann, V. A. (1987) *Biochemistry 26*, 7715–7723.

Haasnoot, C. A. G., den Hartog, J. H. J., de Rooij, J. F. M., van Boom, J. H., & Altona, C. (1980) *Nucleic Acids Res. 8*, 169–181.

Haasnoot, C. A. G., de Bruin, S. H., Berendsen, R. G., Janssen, H. G. J. M., Binnendijk, T. J. J., Hilbers, C. W., van der Marel, G. A., & van Boom, J. H. (1983) *J. Biomol. Struct. Dyn. 1*, 115–129.
Haasnoot, C. A. G., Hilbers, C. W., van der Marel, G. A., van Boom, J. H., Singh, U. C., Pattabiraman, N., & Kollman, P. A. (1986) *J. Biomol. Struct. Dyn. 3*, 843–857.
Hagerman, P. J. (1984) *Proc. Natl. Acad. Sci. U.S.A. 79*, 4632–4636.
Hagerman, P. J. (1990) *Annu. Rev. Biochem. 59*, 755–781.
Hare, D. R., & Reid, B. R. (1986) *Biochemistry 25*, 5341–5350.
Hare, D. R., Wemmer, D. E., Chou, S.-H., Drobny, G., & Reid, B. R. (1983) *J. Mol. Biol. 171*, 319–329.
Ikuta, S., Chattopadhyaya, R., Ito, H., Dickerson, R. E., & Kearns, D. R. (1986) *Biochemistry 25*, 4840–4849.
James, T. L. (1991) *Curr. Opin. Struct. Biol. 1*, 1042–1053.
Joshua-Torr, L., Kabinovich, D., Hope, H., Frolow, F., Appella, E., & Sussman, J. L. (1988) *Nature 334*, 82–84.
Katahira, M., Sugeta, H., Kyogoku, Y., Fujii, S., Fujisawa, R., & Tomita, K. (1988) *Nucleic Acids Res. 16*, 8619–8632.
Katahira, M., Sugeta, H., & Kyogoku, Y. (1990) *Nucleic Acids Res. 18*, 613–618.
Lankhorst, P. P., Haasnoot, C. A. G., Erkelens, C., & Altona, C. (1984) *J. Biomol. Struct. Dyn. 1*, 1387–1405.
Lilley, D. M. J. (1980) *Proc. Natl. Acad. Sci. U.S.A. 77*, 6468–6472.
Macura, S., Huang, Y., Suter, D., & Ernst, R. R. (1981) *J. Magn. Reson. 43*, 259–281.
Miller, M., Harrison, R. W., Wlodawer, A., Appella, E., & Sussman, J. L. (1988) *Nature 334*, 85–86.
Morden, K. M., Chu, Y. G., Martin, F. H., & Tinoco, I., Jr. (1983) *Biochemistry 22*, 5557–5563.
Morden, K. M., Gunn, B. M., & Maskos, K. (1990) *Biochemistry 29*, 8835–8845.
Nadeau, J., & Crothers, D. M. (1989) *Proc. Natl. Acad. Sci. U.S.A. 86*, 2622–2626.
Nelson, H. C. M., Finch, J. T., Luisi, B. F., & Klug, A. (1987) *Nature 330*, 221–226.
Nikonowicz, E., Roongta, V., Jones, C. R., & Gorenstein, D. G. (1989) *Biochemistry 28*, 8714–8725.
Nilges, M., Clore, G. M., Gronenborn, A. M., Brünger, A. T., Karplus, M., & Nilsson, L. (1987) *Biochemistry 26*, 3718–3733.
Nilsson, L., & Karplus, M. (1986) *J. Comput. Chem. 7*, 691–716.
Orbons, L. P. M., van der Marel, G. A., van Boom, J. H., & Altona, C. (1986) *Nucleic Acids Res. 14*, 4187–4196.
Panayotatos, N., & Wells, R. D. (1981) *Nature 289*, 466–470.
Powell, M. J. D. (1977) *Math. Program. 12*, 241–254.
Powers, R., Jones, C. R., & Gorenstein, D. G. (1990) *J. Biomol. Struct. Dyn. 8*, 253–294.
Pramanik, P., Kanhouwa, N., & Kan, L.-S. (1988) *Biochemistry 27*, 3024–3031.
Raghunathan, G., Jernigan, R. L., Miles, H. T., & Sasisekharan, V. (1991) *Biochemistry 30*, 782–788.
Rance, M., Sorensen, O. W., Bodenhausen, G., Wagner, G., Ernst, R. R., & Wüthrich, K. (1983) *Biochem. Biophys. Res. Commun. 117*, 479–485.
Rich, A., & Rajbhandary, U. L. (1976) *Annu. Rev. Biochem. 45*, 805–916.
Rinkel, L. J. & Altona, C. (1987) *J. Biol. Struct. Dyn. 4*, 621–649.
Rinkel, L. J. & Tinoco, I. (1991) *Nucleic Acids Res. 19*, 3695–3700.
Roy, S., Sklenar, V., Appella, E., & Cohen, J. S. (1987) *Biopolymers 26*, 2041–2052.
Sarma, M. H., Gupta, G., & Sarma, R. (1985) *J. Biol. Struct. Dyn. 2*, 1057–1084.
Scheek, R. M., Boelens, R., Russo, N., van Boom, J. H., & Kaptein, R. (1984) *Biochemistry 23*, 1371–1376.
Senior, M. M., Jones, R. A., & Breslauer, K. J. (1988) *Proc. Natl. Acad. Sci. U.S.A 85*, 6242–6246.
Sklenar, V., Miyashiro, H., Zon, G., Miles, T., & Bax, A. (1986) *FEBS Lett. 208*, 94–98.
Tidox, B., Irikura, K., Brooks, B. R., & Karplus, M. (1983) *J. Biomol. Struct. Dyn. 1*, 231–252.
Travers, A. A. (1989) *Annu. Rev. Biochem. 58*, 427–452.
Verlet, L. (1967) *Phys. Rev. 159*, 98–105.
Wang, K. Y., Borer, P. N., Levy, G. C., & Pelczer, I. (1992) *J. Magn. Reson. 96*, 165–170.
Watson, J. D., & Crick, F. H. C. (1953) *Nature 171*, 737–739.
Williamson, J. R., & Boxer, S. G. (1989a) *Biochemistry 28*, 2819–2831.
Williamson, J. R., & Boxer, S. G. (1989b) *Biochemistry 28*, 2831–2836.
Wolk, S. K., Hardin, C. C., Germann, M. W., van de Sande, J. H., & Tinoco, I. (1988) *Biochemistry 27*, 6960–6967.
Wu, H.-M., & Crothers, D. M. (1984) *Nature 308*, 509–513.
Yoon, C., Prive, G. G., Goodsell, D. S., & Dickerson, R. E. (1988) *Proc. Natl. Acad. Sci. U.S.A. 85*, 6332–6336.